




Visualizing spinon Fermi surfaces with time-dependent spectroscopy

Alexander Schuckert ^{1,2,*}, Annabelle Bohrdt ^{1,2,3,4,†}, Eleanor Crane ⁵, and Fabian Grusdt ^{6,2}

¹*Department of Physics and Institute for Advanced Study, Technical University of Munich, 85748 Garching, Germany*

²*Munich Center for Quantum Science and Technology (MCQST), 80799 München, Germany*

³*ITAMP, Harvard-Smithsonian Center for Astrophysics, Cambridge, Massachusetts 02138, USA*

⁴*Department of Physics, Harvard University, Cambridge, Massachusetts 02138, USA*

⁵*Department of Electrical Engineering and London Centre for Nanotechnology, University College London, Gower Street, London WC1E 6BT, United Kingdom*

⁶*Department of Physics and Arnold Sommerfeld Center for Theoretical Physics (ASC), Ludwig-Maximilians-Universität München, Theresienstrasse 37, D-80333 München, Germany*



(Received 9 June 2021; revised 13 November 2021; accepted 15 November 2021; published 6 December 2021)

Quantum simulation experiments have started to explore regimes that are not accessible with exact numerical methods. To probe these systems and enable new physical insights, the need for measurement protocols arises that can bridge the gap to solid-state experiments, and at the same time make optimal use of the capabilities of quantum simulation experiments. Here we propose applying time-dependent photoemission spectroscopy, an established tool in solid-state systems, in cold atom quantum simulators. Concretely, we suggest combining the method with large magnetic field gradients, unattainable in experiments on real materials, to drive Bloch oscillations of spinons, the emergent quasiparticles of spin liquids. We show in exact diagonalization simulations of the one-dimensional t - J model with a single hole that the spinons start to populate previously unoccupied states in an effective band structure, thus allowing us to visualize states invisible in the equilibrium spectrum. The dependence of the spectral function on the time after the pump pulse reveals collective interactions among spinons. In numerical simulations of small two-dimensional systems, spectral weight appears at the ground-state energy at momentum $\mathbf{q} = (\pi, \pi)$, where the equilibrium spectral response is strongly suppressed up to higher energies, indicating a possible route toward solving the mystery of the Fermi arcs in the cuprate materials.

DOI: [10.1103/PhysRevB.104.235107](https://doi.org/10.1103/PhysRevB.104.235107)

I. INTRODUCTION

Just as the back side of the moon is invisible from Earth, certain quantum states may be hidden from standard measurement tools in condensed-matter physics. For example, states may be unoccupied at low temperatures or associated with strongly suppressed matrix elements. Akin to the fascination induced by the back side of the moon in popular culture, the back side of Fermi arcs in the elusive pseudogap phase of cuprate materials has excited condensed-matter physicists for decades.

The cuprates exhibit superconductivity [1] at high temperatures, and fully understanding their phase diagram has become something like a holy grail in the community. One particularly intriguing part of this phase diagram is the pseudogap phase. One of its many fascinating properties is the observation of Fermi arcs in angle-resolved photoemission spectroscopy (ARPES) [2]: around the nodal points $\mathbf{k} = (\pm\pi/2, \pm\pi/2)$, arcs of high spectral weight appear in the spectral function, and in principle they could be part of a small Fermi surface [3,4]. However, these arcs appear to have two end points, and the backside of the putative Fermi surface is invisible. An im-

portant question is thus whether there exist states on the back side of the Fermi arcs, which are invisible in ARPES measurements. If this is the case, Luttinger's theorem [5] would be violated, as the area enclosed by the putative Fermi surface would be too small, indicating either a thus far unknown broken translational symmetry or topological excitations [6].

Here we propose a scheme to probe unoccupied states [7–9] in the spectral function of strongly correlated many-body systems, realizable in quantum simulators. It is based on pump-probe spectroscopy, which has recently emerged as a valuable tool in solid-state experiments to study nonequilibrium properties of materials [10–15]. Quantum simulators such as ultracold atoms have several advantages: for example, the absence of phonons leads to long coherence times, and the Hamiltonian parameters are well known and tunable. In particular, a different toolbox for possible probe pulses is available, such as magnetic field gradients with strengths unattainable in solid-state experiments. For these reasons, our scheme is an important complement to existing pump-probe experiments. Our proposal to implement time-dependent ARPES (td-ARPES) to visualize spinon states in cold atoms is within reach of current quantum gas microscopy experiments, which have recently realized all the required building blocks: a magnetic field gradient [16], angle-resolved photoemission spectroscopy [17–19], and Bloch oscillations [20–22].

*alexander.schuckert@tum.de

†annabelle.bohrdt@cfa.harvard.edu

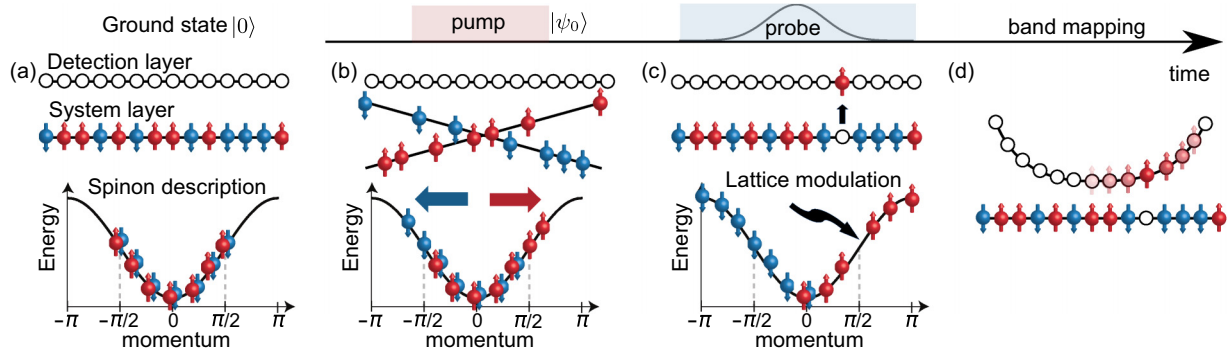


FIG. 1. Time-dependent photoemission spectroscopy in quantum gases. (a) A half-filled 1D Fermi-Hubbard chain in the ground state, corresponding to a spinon Fermi sea, is prepared in the system layer while the detection layer is empty. (b) A strong magnetic field gradient is applied, leading to Bloch oscillations in opposite directions of the two spinon species. (c) After the field is switched off, a weak lattice modulation is applied, exciting an atom to the detection layer. (d) Finally, the momentum of the excited atom in the detection layer is measured, e.g., in a harmonic potential by a quarter-period oscillation, using time-of-flight or another adiabatic band-mapping scheme.

Applying our td-ARPES scheme to the Fermi-Hubbard model, which has been realized with cold atoms in several quantum gas microscopes [16,23–25], directly enables the study of fractionalized excitations: In the one-dimensional (1D) Fermi-Hubbard model, the electron is effectively split into *independent* charge and spin excitations, called chargin and spinon, respectively [26–28]. The single-particle spectra of the 1D Fermi-Hubbard and t - J models exhibit a strong asymmetry [29], which can be associated with the fermionic statistics of spinons and their Fermi sea [30].

Here, we demonstrate by numerical simulations that td-ARPES combined with strong external field gradient pulses can shed light on spinon states not occupied in the ground state of the half-filled 1D t - J model, up to the highest momentum $k = \pi$; see Fig. 1. In two dimensions, we show that a magnetic field gradient pulse along the diagonal direction yields spectral weight at low energies at $k = (\pi, \pi)$. While we focus on the ARPES spectrum of the half-filled ground state, i.e., the properties of a single hole inserted into the spin system, this provides a hint that the missing weight on the back side of the Fermi arcs may be related to a spinon Fermi sea picture [31] even at finite doping.

II. TIME DEPENDENT SPECTROSCOPY IN QUANTUM SIMULATORS

Our protocol combines the equilibrium ARPES protocol [19,30] for quantum simulators with the solid-state td-ARPES protocol [32,33]. First, a system in equilibrium is prepared in one layer of an optical lattice. A neighboring layer (“detection layer”) is left empty with a gradient along the transverse direction inhibiting tunneling between the layers due to the energy difference Δ induced by the gradient; see Fig. 1(a). Subsequently, a nonequilibrium state $|\psi_0\rangle$ is prepared by a quench, such as the application of an external field. Here, we propose to apply a strong magnetic field gradient for a time t_B ; see Fig. 1(b). Magnetic field gradients have been realized in

quantum gas microscopy experiments, for example, to study spin transport [16].

To measure the time-dependent ARPES spectrum $A_{\mathbf{q}}(T, \omega)$, we suggest to apply a weak lattice modulation between system and detection layers with frequency $\tilde{\omega}$ and a Gaussian envelope centered around time T with variance Σ^2 ; see Fig. 1(c). In the weak modulation limit, this allows a single atom of energy $\epsilon_{\mathbf{q}}$ and spin σ to tunnel resonantly into the detection layer if $\tilde{\omega} = \epsilon_{\mathbf{q}} + \Delta$. Alternatively to the detection layer, a noninteracting third hyperfine state can be used, with the lattice modulation replaced by a radiofrequency (rf) pulse [19]. This enables the application of our protocol in continuum quantum gases, where rf spectroscopy in equilibrium is routinely performed [34–36].

Finally, one of the band-mapping schemes described in [30] can be used to measure the momentum of the atom in the detection layer at long times after the pulse has subsided, i.e., $t \gg T + \Sigma$; see Fig. 1(d). We show in Appendix A that the momentum space occupation number in the detection layer is proportional to the time-dependent hole spectral function $A_{\mathbf{q}\sigma}(T, \omega)$,

$$A_{\mathbf{q}\sigma}(T, \omega) = \int d\tau e^{i\omega\tau} \langle \hat{c}_{\mathbf{q},\sigma}^\dagger(T + \tau/2) \hat{c}_{\mathbf{q},\sigma}(T - \tau/2) \rangle, \quad (1)$$

at frequency $\omega = \tilde{\omega} - (\epsilon_{\mathbf{q}} + \Delta)$ and central time T . The expectation value is evaluated with respect to the initial state. Here, $\hat{c}_{\mathbf{q},\sigma}^{(\dagger)}$ annihilates (creates) a fermion or boson of spin σ and momentum \mathbf{q} . The particle spectral function $\int d\tau e^{i\omega\tau} \text{Tr}(\rho \hat{c}_{\mathbf{q}\sigma}(T + \tau/2) \hat{c}_{\mathbf{q}\sigma}^\dagger(T - \tau/2))$ can be measured by the same protocol by initially preparing the detection layer in a band-insulator; see Appendix A. The modulation leads in this case to an assisted tunneling of an atom from the detection layer into the system, whose momentum can be obtained by band-mapping of the resulting hole in the detection layer. In the solid state, this protocol is known as angle-resolved inverse-photoemission spectroscopy (ARIPES) [37]. Note that ARIPES does not give new information to ARPES in the half-filled Hubbard model due to its particle hole

symmetry, hence we cannot rely on this technique to study unoccupied states in our case.

III. OCCUPYING HIGHER MOMENTUM SPINON STATES BY BLOCH OSCILLATIONS

Here, we use our tdARPES protocol to probe unoccupied spinon states in the t - J model,

$$\hat{H}_{t,J} = -t \sum_{\langle i,j \rangle, \sigma} \mathcal{P}(\hat{c}_{i,\sigma}^\dagger \hat{c}_{j,\sigma} + \text{H.c.})\mathcal{P} + J \sum_{\langle i,j \rangle} \hat{S}_i \cdot \hat{S}_j, \quad (2)$$

where \mathcal{P} denotes projection on the Hilbert space without double occupancies, $\langle i, j \rangle$ denotes neighboring sites, and \hat{S}_j are spin-1/2 operators.

The 1D t - J model exhibits spin-charge separation [26]. This can be made explicit by writing the original fermionic operators as $\hat{c}_{i,\sigma} = \hat{h}_i^\dagger \hat{f}_{i,\sigma}$, where the spin operators \hat{S}_i are related to the fermionic spinon operators as $\hat{S}_i = \frac{1}{2} \sum_{\alpha,\beta} \hat{f}_{i,\alpha}^\dagger \sigma_{\alpha,\beta} \hat{f}_{i,\beta}$, and \hat{h}_i denotes the bosonic chargin operator [38,39]. On a mean-field level, the time-dependent spectral function can be approximated as a convolution of spinon and chargin contribution,

$$A_{q\sigma}(T, \omega) = \sum_{k_h} \int d\nu A_{q-k_h\sigma}^s(T, \omega - \nu) A_{k_h}^c(T, \nu). \quad (3)$$

This representation serves in particular to determine the positions at which spectral weight should appear as it explicitly satisfies momentum and energy conservation. Note that due to spin-charge separation, the chargin can be approximated as a fully occupied free particle with dispersion $\epsilon_h(k) = -2t \cos(k)$ when $t \gg J$ [40], i.e.,

$$A_k^c(\nu) = 2\pi \delta(\omega + 2t \cos(k)). \quad (4)$$

To gain a better understanding of the spinon contribution to the spectrum, we express the spin part of the Hamiltonian in Eq. (2) in terms of the spinons [41]:

$$\hat{H}_J = -\frac{1}{2} \sum_{\langle i,j \rangle, \alpha} \hat{f}_{i,\alpha}^\dagger \hat{f}_{j,\alpha} [J_\perp \hat{f}_{j,\bar{\alpha}}^\dagger \hat{f}_{i,\bar{\alpha}} + J_z \hat{f}_{j,\alpha}^\dagger \hat{f}_{i,\alpha}], \quad (5)$$

where $\bar{\uparrow} = \downarrow$ and $\bar{\downarrow} = \uparrow$. This expression is exact within the subspace satisfying $\sum_\alpha \hat{f}_{i,\alpha}^\dagger \hat{f}_{i,\alpha} = 1$ [30,41].

In a mean-field description of the SU(2) invariant model with $J_\perp = J_z$, we replace the operator $\hat{f}_{i,\alpha}^\dagger \hat{f}_{j,\alpha}$ by its ground-state expectation value, leading to the formation of a Fermi sea of the spinons $\hat{f}_{i,\sigma}$ [30]. In standard ARPES, fermions can only be removed from formerly occupied states, and thus spectral weight only appears for spinon momenta within the Fermi sea. For an undoped spin chain, this corresponds to $k_F = \pm\pi/2$. At momenta $|k| > \pi/2$, states of the many-body system exist, but they are not occupied and therefore they do not yield any weight in the spectral function.

Here, we want to probe these unoccupied spinon states of the 1D t - J model at zero temperature by driving the system out of equilibrium before measuring the time-dependent one-hole ARPES spectrum, akin to solid-state pump-probe experiments. We do so by applying a magnetic field gradient,

described by the Hamiltonian

$$\hat{H}_B = -B \sum_j j \hat{S}_j^z, \quad (6)$$

for a time t_B , starting from the $B = 0$ ground state. Numerically, we consider periodic boundary conditions for a cleaner signal, and we apply a time-dependent unitary transformation in order to restore translational invariance; see Appendix B. After time t_B , we switch the gradient field off and calculate the td-ARPES spectrum of the resulting nonequilibrium state with exact diagonalization.

In the slave particle mean-field picture, we find (see Appendix C)

$$A_{k,\alpha}^s(\omega) = 2\pi \delta\left(\omega + \frac{2J}{\pi} \cos(k)\right) \Theta\left(|k + \alpha B t_B / 2| - \frac{\pi}{2}\right), \quad (7)$$

corresponding to the spectral function of free fermions with dispersion $-\frac{2J}{\pi} \cos(k)$, occupying a Fermi sea centered around a nonzero momentum determined by the magnetic field. Hence, the magnetic field gradient exerts an equal but opposite force on the two spinon species, shifting their occupation along the mean-field spinon dispersion. The duration t_B is chosen such that these Bloch oscillations lead to a total shift $\theta = B t_B$, such that after the application of the magnetic field, states with momentum $-\pi/2 \mp \theta/2 \leq k \leq \pi/2 \mp \theta/2$ are occupied by up and down spinons, respectively. The spinons only experience half the total shift since Eq. (6) introduces a coupling of $\mp B/2$ to the density of up/down spinons.

The resulting spinon spectrum therefore reveals the shifted Fermi seas: spectral weight is obtained for momenta q which are now occupied and were previously empty in the ground state. Within mean-field theory, the positions of spectral lines can be obtained by inserting the known spinon and chargin dispersions [26,42,43] into Eq. (3), a procedure known as the spectral building principle.

In Fig. 2, we show the numerically obtained spectral function after applying a magnetic field gradient pulse of different strengths, yielding different shifts $\theta/2$. We always remove a spin-down particle, thus probing only one of the two spinon Fermi seas. Comparing the numerical results to the spectral building principle [42,43]—where shifts due to the magnetic field gradient are explicitly taken into account—yields perfect agreement, providing strong evidence that the slave-particle mean-field theory remains an accurate description beyond the ground state. However, while the mean-field picture predicts a shift of spectral weight in only one direction along the dispersion by $+\theta/2$, we find weight appearing on *both* sides at $\pm\theta/2$. In the following, we show that this is due to a time dependence of the spectrum induced by interactions among spinons.

IV. COHERENT OSCILLATIONS OF THE SPECTRUM

In the slave-particle mean-field theory, the shifted Fermi sea is still an eigenstate of the Hamiltonian, and we thus do not expect to find any dependence on the central time T . For sufficiently small magnetic field gradients, the spectral function $A_{q\sigma}(T, \omega)$ indeed does not exhibit a dependence on T . However, if the magnetic field gradient is strong, with

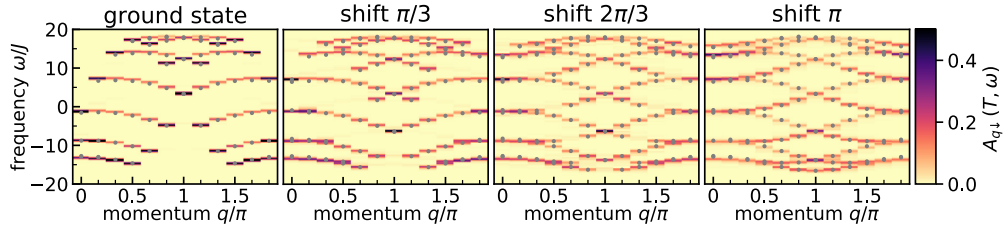


FIG. 2. Occupying spinon states by magnetic field gradient pulses. The nonequilibrium one-hole spectral function obtained from exact diagonalization for a system with $L = 12$ sites at $t/J = 8$ is shown after a magnetic field gradient was applied. The shift in momentum space is given by the product of magnetic field strength and duration of the gradient, $\theta = Bt_B$, with $t_B = 10/J$. Gray dots denote the points where spectral weight is expected from the mean-field theory spectral building principle, Eq. (3). The momentum shift due to the magnetic field gradient has been explicitly taken into account in the spinon properties while the chargin stays unaffected. Central times shown are $JT = 12.5, 15, 15$ for shift $\theta = \pi/3, 2\pi/3, \pi$.

$B \sim J$, coherent oscillations of the spectral weight emerge, Fig. 3; see also the video in the supplementary data [44].

In particular, the spectral weight in momentum space oscillates between the occupied momenta for up and down spinons, with the spectra for up and down fermions oscillating exactly out of phase; see Figs. 3(g)–3(i). However, the position of the spectral lines does not change. This is most clearly visible when considering the lowest branch with a fixed holon momentum. There, the two extremal points of the branch have a strong weight at opposite extrema of the oscillations, indicating occupation of the spinon energies at each side of the Fermi sea.

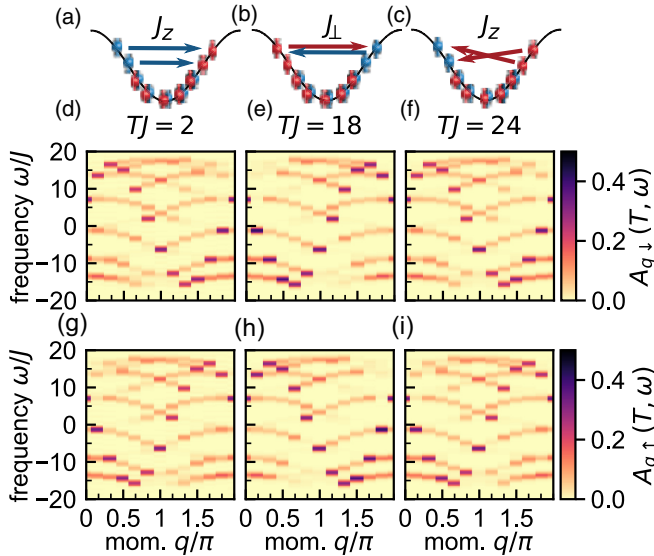


FIG. 3. Coherent oscillations of the spectral weight. (a)–(c) Resonant scattering processes leading to a redistribution of spectral weight between the shifted mean-field Fermi surfaces. (d)–(f) The spectral function $A_{q\downarrow}(T, \omega)$ from exact diagonalization is shown as a function of momentum and frequency for three central times T in a system with $L = 12$ sites for the case of shift $2\pi/3$ shown in Fig. 2. Comparing the spectral function at different central times shows the oscillations of the spectral weight from one side of the visible arcs to the other, corresponding to the Fermi surfaces of the up and down spinon Fermi seas. (g)–(i) same as in (d)–(f) but for the spectrum of \uparrow fermions, showing that it oscillates exactly out of phase with the \downarrow spectrum.

We can further analyze the spectrum by using the decomposition of the Lehmann representation of the spectral function into time-dependent and thermal parts according to

$$A_{q\sigma}(T, \omega) = A_{q\sigma}^{\text{th}}(\omega) + A_{q\sigma}^{\text{td}}(T, \omega) \quad (8)$$

with

$$A_{q\sigma}^{\text{th}}(\omega) = \sum_n |\langle \psi_0 | n^N \rangle|^2 \sum_l |\langle l^{N-1} | c_{q\sigma} | n^N \rangle|^2 \times \delta(\omega - (E_l^{N-1} - E_n^N)), \quad (9)$$

$$A_{q\sigma}^{\text{td}}(T, \omega) = \sum_{n, m \neq n} \langle \psi_0 | n^N \rangle \langle m^N | \psi_0 \rangle e^{i(E_n^N - E_m^N)T} \times \sum_l \langle n^N | c_{q\sigma}^\dagger | l^{N-1} \rangle \langle l^{N-1} | c_{q\sigma} | m^N \rangle \times \delta\left(\omega - E_l^{N-1} + \frac{E_m^N + E_n^N}{2}\right). \quad (10)$$

A^{th} is the expected steady-state spectral function from the diagonal ensemble. The only time dependence is contained in the phase factors in A^{td} . Remarkably, they only depend on eigenstates with occupation N , i.e., the system before inserting a hole. In our case, this corresponds to the ground state of the undoped t - J model, i.e., the Heisenberg spin system. This shows that the only dependence on the time T enters through the eigenstates of the *half-filled* system without a hole, which is an exact result. Employing our mean-field spinon picture of the ground state of the Heisenberg model, this time dependence of the spectral function indicates a new route to probe the properties of the spinons in the Heisenberg model.

Beyond mean-field interactions lead to oscillations

Since the time dependence observed in the spectrum goes beyond a mean-field description, we conclude that interactions between the spinons are relevant; see also [45]. To understand this effect in more detail, we examine the quartic slave-particle Hamiltonian in Eq. (5). First, we consider the J_z term in the Hamiltonian, reading $-J_z/(2L) \sum_{\sigma, q, k, k'} \cos(q) \hat{f}_{k+q\sigma}^\dagger \hat{f}_{k'-q\sigma}^\dagger \hat{f}_{k'\sigma} \hat{f}_{k\sigma}$ in momentum space. Enforcing energy conservation on the level of the mean-field dispersion, only processes involving $q = 0$, $k' = \pi - k$, or $k' = q + k$ are allowed, examples of which are

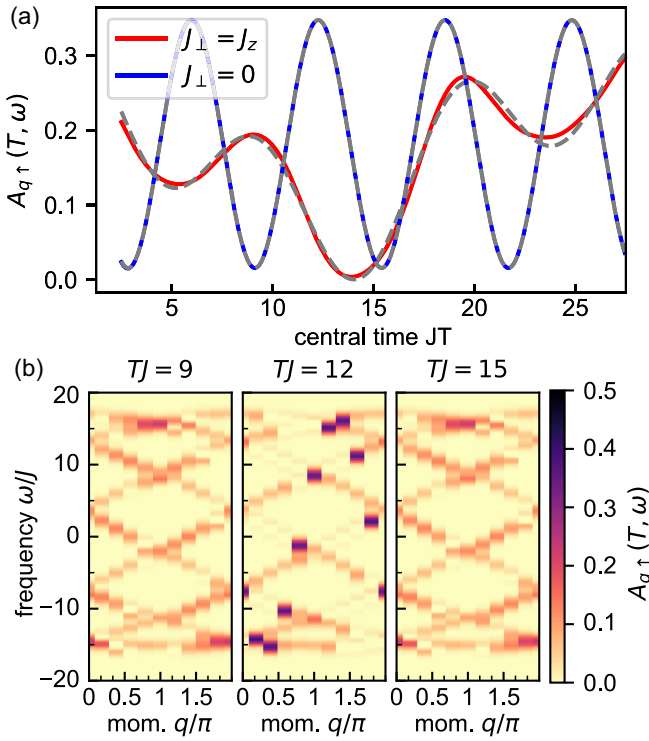


FIG. 4. Comparing coherent oscillations of the spectrum with and without J_{\perp} . (a) Central time dependence of the spectral line with the lowest frequency ($\omega \approx -15.58$) for momentum $q = 4\pi/L$. Gray dashed lines indicate a fit with a single sine function with frequency $\approx 1J_z$ for $J_{\perp} = 0$ and a sum of two sine functions with frequencies $0.25J$ and $0.64J$ for $J_{\perp} = J_z = J$. (b) Snapshots of the spectrum at the maxima and minima of the oscillations for $J_{\perp} = 0$. $L = 10$, $t = 8J$. Total shift $\Theta = 2 \times 2\pi/L$. Data from exact diagonalization.

sketched in Figs. 3(a) and 3(c). An indication for the validity of this picture is obtained considering a shift by a single momentum point, $\Theta = 4\pi/L$. In this case, there are only very few processes allowed by the spinon Hamiltonian when imposing both momentum and energy conservation. This becomes particularly extreme in the case when $J_{\perp} = 0$. Then, only one state has the same energy as the shifted Fermi sea and is also connected to the shifted Fermi sea by a momentum-conserving process: its “conjugate” partner, i.e., the Fermi sea shifted in the opposite direction in momentum space. Within this picture, the spectrum is expected to perform Rabi oscillations between the shifted Fermi sea and its conjugate partner. In Fig. 4 we show the time evolution of the spectrum when switching $J_{\perp} = 0$ after t_B . The Fermi sea then performs perfect sinusoidal oscillations with frequency J_z , as we show by considering the spectral weight of a single line (all others perform the same oscillations). This supports the picture discussed above. However, when looking at snapshots of the whole spectrum, we see that the conjugate state is never fully reached, which may be attributed to a detuning between the shifted Fermi sea and its conjugate introduced by non-energy-conserving processes not included in this picture. Contrarily, when keeping $J_{\perp} = J_z$, we find an oscillation with a superposition of two sine functions, which we attribute to the coupling of the two oscillating Fermi seas by J_{\perp} .

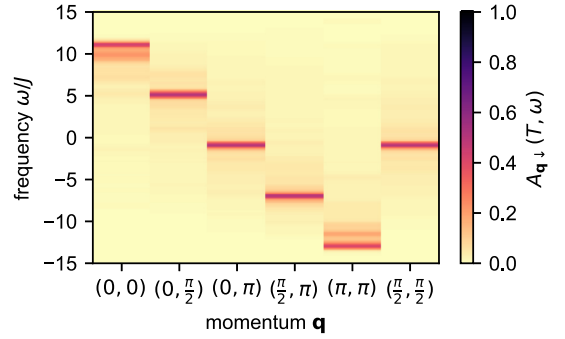


FIG. 5. Emergence of the free-particle spectrum for (π, π) shift in 2D. Here, we use $t = 3J$ as well as $t_B = 1/J$. Data from exact diagonalization.

In summary, we have shown that coherent oscillations between the two shifted Fermi seas are present, which we attributed to beyond mean-field interactions between spinons.

V. TWO-DIMENSIONAL t - J MODEL

The same protocol can also be applied in a 2D system. In Fig. 6, we show numerical results for the spectral function $A_{q\downarrow}(T, \omega)$ in the t - J model on a 4×4 torus at momentum $\mathbf{q} = (\pi, \pi)$. In equilibrium, the spectral weight is strongly suppressed at this momentum at low energies. A possible explanation involves binding of a light charged to a heavy fermionic spinon from a Fermi sea [31]. This suggests that additional spectral weight should appear at low energies when the magnetic field gradient is switched on and the putative spinon Fermi surface is displaced.

When employing a very strong magnetic field gradient with pulse duration $t_B < 1/J$ and total shift $\Theta = (\pi, \pi)$, we find the spectrum to be identical to the one of a free particle hopping with dispersion $-2t(\cos(q_x) + \cos(q_y))$; see Fig. 5. We can explain this by considering the strong magnetic field gradient limit, in which we can neglect the Heisenberg Hamiltonian during the dynamics, and the system only evolves due to the gradient field. The initial state of the dynamics is given by the ground state of the Heisenberg model in 2D, which shows antiferromagnetic correlations. Now, a (π, π) pulse corresponds to a spin flip operator on every second site around the z axis, such that in the xy plane, there are now ferromagnetic correlations. In a ferromagnet, an injected hole can move freely as there is no energy cost related to the reshuffling of spins associated with the movement of the hole. Hence, the spectrum becomes identical to the one of a free particle.

In the less extreme regime of moderately long t_B and $\theta = \pi/2$, the magnetic field gradient leads to the appearance of spectral weight around the ground-state energy of a single hole in the t - J model, indicated by arrows in Fig. 6. We interpret this feature as a signature of the occupation of unoccupied states of a spinon Fermi sea in two dimensions, in analogy to the one-dimensional case discussed above. Moreover, a high-energy feature around $\omega \approx 5$ appears for the same values of t_B at which the low-energy feature appears. Finally, for very slow quenches, finite-size gaps prevent any interesting dynamics, and the obtained spectrum resembles the ground-state result.

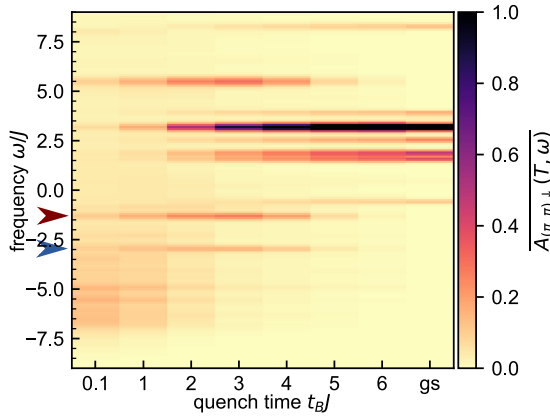


FIG. 6. Time-dependent ARPES in two dimensions. The spectral function $A_{\mathbf{q}_l}(T, \omega)$ in the t - J model on a 4×4 torus at $t/J = 2$ evaluated at momentum $\mathbf{q} = (\pi, \pi)$ calculated for a magnetic field gradient along the diagonal of strength $Bt_B = \pi/2$ for different quench times t_B . We average over central times $10 \leq JT \leq 20$, indicated by the overline. The magnetic polaron ground-state (gs) energy at momentum $q = (\pi, \pi)$ [$q = (\pi/2, \pi/2)$], $\omega \approx -2.93J$ ($\omega \approx -1.28J$) is indicated by a red (blue) arrow. Data from exact diagonalization.

VI. SUMMARY AND OUTLOOK

We propose a measurement scheme to reveal unoccupied spinon states in the one-hole spectral function. Our numerical results for the 1D t - J model show that a strong magnetic field gradient leads to spinon Bloch oscillations, where the spinons occupy previously empty momentum states. These can then be probed by time-dependent spectroscopy, revealing beyond mean-field interactions among spinons. Extending our results to small 2D systems, we are able to visualize the ground state of the magnetic polaron at momentum $\mathbf{q} = (\pi, \pi)$ in the spectral function, which has no spectral weight in the equilibrium spectrum [31].

A promising future direction is to perform similar numerical simulations of the time-dependent spectral function for extended 2D systems. The perhaps most interesting candidates are the 2D Fermi-Hubbard or t - J models at finite doping, where our protocol can help to resolve the long-standing question concerning the existence of (unoccupied) states on the back side of the Fermi arcs. As numerical calculations in this regime are challenging, experimental realizations become essential. Measuring the particle spectral function, which is challenging in solids, could lead to an alternative route to probing unoccupied states. Apart from the square lattice t - J model discussed here, pump-probe spectroscopy with strong magnetic fields also enables new insights into the properties of spinons in other models and geometries, such as triangular and kagomé lattices or the J_1 - J_2 model [46]. Graphene, simulable in hexagonal lattice quantum simulators, exhibits a d -wave superconducting state due to a Van Hove singularity, which could be probed by shifting the band-structure occupation akin to our protocol [47].

Our quench protocol, combining magnetic field gradients with ARPES, could be complemented by other techniques in future pump-probe experiments in cold atoms. In particular, two-photon photoemission is an established technique in the

solid state to probe unoccupied states by creating a dipole before photoemission [48]. Moreover, while difficult to implement in the solid state, ARIPES could be used in cold atoms. Lastly, combining different synthetic field pumps, including spin-independent gradient fields (the analog of electric fields) and strong magnetic fields [49], might help to distinguish charge and spin dynamics as well as topological effects in the regime of finite doping.

ACKNOWLEDGMENTS

We thank Michael Knap for fruitful discussions and comments, and we acknowledge useful discussions with Nir Navon, Eugene Demler, Daniel Greif, Waseem Bakr, Christian Gross, and Immanuel Bloch. We acknowledge support from the Deutsche Forschungsgemeinschaft (DFG, German Research Foundation) under Germany's Excellence Strategy-EXC-2111-390814868, the Max Planck Gesellschaft (MPG) through the International Max Planck Research School for Quantum Science and Technology (IMPRS-QST), the NSF through a grant for the Institute for Theoretical Atomic, Molecular, and Optical Physics at Harvard University, the Smithsonian Astrophysical Observatory, and the UK Engineering and Physical Sciences Research Council (COMPASSS/ADDRFSS, Grant No. EP/M009564/1).

A.S. and A.B. contributed equally to this work.

APPENDIX A: DETAILS ON THE SPECTROSCOPY PROTOCOLS

Here we derive the explicit expressions for the spectroscopy protocols discussed in the main text.

1. Linear and quadratic response

Consider a system with many-body Hamiltonian \hat{H}_0 and probe Hamiltonian \hat{V} (e.g., containing a lattice modulation or rf pulse), such that the total Hamiltonian is given by $\hat{H} = \hat{H}_0 + \hat{V}$. We work in an interaction picture with respect to \hat{H}_0 such that operators are evolved according to $\hat{A}_I(t) = \hat{U}_0^\dagger(t) \hat{A} \hat{U}_0(t)$, with $\hat{U}_0(t) = \mathcal{T} \exp(-i \int dt' \hat{H}_0(t'))$. The initial density matrix $\hat{\rho}_0$ is evolved according to $\hat{\rho}(t) = \hat{U}(t) \hat{\rho}_0 \hat{U}^\dagger(t)$ with $\hat{U}(t) = \mathcal{T} \exp(-i \int_0^t \hat{V}_I(t') dt')$. Up to second order in \hat{V} , the time evolution operator is given by

$$\hat{U}(t) = \mathbb{1} - i \int_0^t dt_1 \hat{V}_I(t_1) - \int_0^t dt_1 \int_0^{t_1} dt_2 \hat{V}_I(t_1) \hat{V}_I(t_2) + O(V^3). \quad (\text{A1})$$

The expectation value of an observable \hat{A} at time t , $\langle \hat{A}(t) \rangle \equiv \text{Tr}(\hat{\rho}(t) \hat{A}_I(t))$, is then given by

$$\begin{aligned} \langle \hat{A}(t) \rangle - \langle \hat{A}(t) \rangle_{V=0} &= -i \int_0^t dt_1 \langle [\hat{A}_I(t), \hat{V}_I(t_1)] \rangle \\ &+ \int_0^t dt_1 \int_0^{t_1} dt_2 \langle \hat{V}_I(t_1) \hat{A}_I(t) \hat{V}_I(t_2) \rangle \end{aligned}$$

$$\begin{aligned}
& - \int_0^t dt_1 \int_0^{t_1} dt_2 \langle \hat{V}_I(t_2) \hat{V}_I(t_1) \hat{A}_I(t) \rangle \\
& - \int_0^t dt_1 \int_0^{t_1} dt_2 \langle \hat{A}_I(t) \hat{V}_I(t_1) \hat{V}_I(t_2) \rangle + O(V^3), \quad (\text{A2})
\end{aligned}$$

where $\langle \hat{A}(t) \rangle_{V=0}$ is the expectation value in the absence of a probe pulse.

The above expression is valid for any density matrix $\hat{\rho}_0$, in particular also for thermal equilibrium $\hat{\rho}_0 = \frac{1}{Z} e^{-\beta \hat{H}_0}$ with $Z = \text{Tr}(e^{-\beta \hat{H}_0})$.

2. Time-dependent ARPES

In the following, we specify the above very general expressions for our specific physical situation. The protocol consists in coupling the “system” optical lattice to another tube/layer representing a “detection” lattice, which is initially empty. The detection lattice is offset by an energy Δ , which is the analog of the work function in condensed matter ARPES. An analog of a photopulse is created by modulating the lattice depth between system and detection layer, resulting in a coupling Hamiltonian

$$\hat{V}_I(t) = -t_y s(t) e^{-i\omega t} \sum_{\mathbf{k}} \hat{d}_{\mathbf{k}\sigma}^\dagger \hat{c}_{\mathbf{k}\sigma} + \text{H.c.}, \quad (\text{A3})$$

$$\langle \hat{n}_{\mathbf{q}\sigma}(t) \rangle = t_y^2 \int_0^t dt_1 \int_0^{t_1} dt_2 s(t_1) s(t_2) \sum_{\mathbf{k}'\mathbf{k}'', \sigma'\sigma''} \langle 0 | \hat{d}_{\mathbf{k}'\sigma'}^\dagger(t_1) \hat{n}_{\mathbf{q}\sigma}(t) \hat{d}_{\mathbf{k}''\sigma''}^\dagger(t_2) | 0 \rangle \text{Tr}(\hat{\rho}_s \hat{c}_{\mathbf{k}'\sigma'}^\dagger(t_1) \hat{c}_{\mathbf{k}''\sigma''}(t_2)) e^{i\omega(t_1-t_2)} \quad (\text{A4})$$

$$= t_y^2 \int_0^t dt_1 \int_0^{t_1} dt_2 s(t_1) s(t_2) e^{i(\omega - \epsilon_{\mathbf{q}} - \Delta)(t_1 - t_2)} \text{Tr}(\hat{\rho}_s \hat{c}_{\mathbf{q}\sigma}^\dagger(t_1) \hat{c}_{\mathbf{q}\sigma}(t_2)) \quad (\text{A5})$$

$$= t_y^2 \int_0^t dT \int_{-\tau_{\max}(T)}^{\tau_{\max}(T)} d\tau s\left(T - \frac{\tau}{2}\right) s\left(T + \frac{\tau}{2}\right) e^{i(\omega - \epsilon_{\mathbf{q}} - \Delta)\tau} A(T, \tau), \quad (\text{A6})$$

where we defined the center-of-mass time $T = \frac{1}{2}(t_1 + t_2)$, and relative time τ as well as the “lesser” Green’s function $A(T, \tau) = \text{Tr}(\hat{\rho}_s \hat{c}_{\mathbf{q}\sigma}^\dagger(T + \tau/2) \hat{c}_{\mathbf{q}\sigma}(T - \tau/2))$. The maximum relative time is $\tau_{\max} = 2T$ for $T \leq t/2$ and $\tau_{\max} = 2t$ for $T > t/2$. In most situations, however, we can send $\tau_{\max} \rightarrow \infty$ due to the rapid decay of $A(T, \tau)$. We note that this expression is valid for both fermionic and bosonic species because we assumed the detection system to be initially empty.

3. Special pulses for tdARPES protocol

In the following, we will discuss a few instructive limits of the above general expression.

a. Equilibrium limit

We can recover the equilibrium result of Ref. [30] by inserting $s(t) = 1$ as well as using that in equilibrium, $\hat{\rho}_s = \frac{1}{Z} e^{-\beta \hat{H}_0}$, $A(T, \tau)$ only depends on τ . The rate of tunneling to the detection system is then given by

$$\Gamma_{\mathbf{q}\sigma}(\omega) = \frac{1}{t} \langle \hat{n}_{\mathbf{q}\sigma}(t) \rangle \quad (\text{A7})$$

$$= t_y^2 \int_{-\infty}^{\infty} dt e^{i(\omega - \epsilon_{\mathbf{q}} - \Delta)t} \frac{1}{Z} \text{Tr}(e^{-\beta \hat{H}_0} \hat{c}_{\mathbf{q}\sigma}^\dagger(t) \hat{c}_{\mathbf{q}\sigma}) \quad (\text{A8})$$

where $\hat{d}_{\mathbf{k}\sigma}^\dagger, \hat{c}_{\mathbf{k}\sigma}$ creates/annihilates an atom with spin σ in the detection/system layer; t_y is the amplitude of the modulation, which needs to be small compared to the tunneling within the system; and ω is the modulation frequency. The detection system is assumed to be noninteracting, such that $\hat{H}_d = \sum_{\mathbf{q}} (\epsilon_{\mathbf{q}} + \Delta) \hat{d}_{\mathbf{q}\sigma}^\dagger \hat{d}_{\mathbf{q}\sigma}$, with $\epsilon_{\mathbf{q}}$ the noninteracting dispersion of the detection lattice. The operator measured in this scheme is the momentum space occupation number in the detection system $\hat{A} = \hat{n}_{\mathbf{q}\sigma} \equiv \hat{d}_{\mathbf{q}\sigma}^\dagger \hat{d}_{\mathbf{q}\sigma}$, which may be obtained from the band-mapping schemes in Ref. [30]. The total initial density matrix $\hat{\rho}_0$ is a product state of the empty detection system and the system density matrix $\hat{\rho}_0 = |0\rangle \langle 0|_d \otimes \hat{\rho}_s$.

Inserting $\hat{A} = \hat{n}_{\mathbf{q}\sigma}(t)$ into Eq. (A2), we directly see that the linear term in \hat{V}_I vanishes as it contains a vacuum expectation value of an odd number of detection system creation/annihilation operators. Furthermore, the terms in the second line of Eq. (A2) also vanish, as $\hat{A}_I(t) = \hat{n}_{\mathbf{q}\sigma}(t)$ acting on the empty detection initial state gives zero. Moreover, in the absence of system-detection layer tunneling, the occupation number in the detection system remains zero, such that $\langle \hat{n}_{\mathbf{q}\sigma}(t) \rangle_{t_y=0} = 0$ at all times. The last remaining term then finally gives

$$= t_y^2 A_{\mathbf{q}\sigma}(\omega - \epsilon_{\mathbf{q}} - \Delta). \quad (\text{A9})$$

$A_{\mathbf{q}\sigma}(\omega)$ is the hole spectral function

$$A_{\mathbf{q}\sigma}(\omega) = \frac{1}{Z} \sum_{nm} e^{-\beta E_n} |\langle m | \hat{c}_{\mathbf{k}\sigma} | n \rangle|^2 \delta(\omega - (E_m - E_n)). \quad (\text{A10})$$

b. Gaussian pulse

A (normalized) Gaussian pulse centered around $t = t_p$ as $s(t) = \frac{1}{\sqrt{2\pi\sigma^2}} \exp(-\frac{(t - t_p)^2}{2\sigma^2})$ leads to

$$\begin{aligned}
2\pi\sigma^2 \langle \hat{n}_{\mathbf{q}\sigma}(t) \rangle &= \int_0^t dT \int_{-T}^T d\tau \exp\left(-\frac{(T - t_p)^2}{\sigma^2}\right) \\
&\times \exp\left(-\frac{\tau^2}{8\sigma^2}\right) e^{i(\omega - \epsilon_{\mathbf{q}} - \Delta)\tau} A(T, \tau). \quad (\text{A11})
\end{aligned}$$

Typically, $A(T, \tau)$ decays rapidly as a function of τ (with the decay rate corresponding to the lifetime of excitations in the system), such that we can extend the integral boundaries for the τ integral to $\pm\infty$. Then we can interpret the τ integral as a Fourier transform, with a broadening introduced by the finite

pulse length, leading to

$$\begin{aligned} \langle \hat{n}_{\mathbf{q}\sigma}(t) \rangle &= \sqrt{\frac{2}{\pi\sigma^2}} \int_0^t dT \exp\left(-\frac{(T-t_p)^2}{\sigma^2/2}\right) \\ &\times \int \frac{d\tilde{\omega}}{2\pi} \exp(-2\sigma^2\tilde{\omega}^2) A(T, \omega - \epsilon_{\mathbf{q}} - \Delta - \tilde{\omega}). \end{aligned} \quad (\text{A12})$$

Hence, a Gaussian pulse centered around t_p measures the time-dependent lesser Green's function averaged over a time and frequency window fulfilling the ‘‘uncertainty relation’’ $\sigma_T^2\sigma_\omega^2 = \frac{1}{16}$.

4. Time-dependent ARIPES

To measure the ARIPES spectrum, we propose to prepare the detection layer in a band insulator, i.e., all momenta are initially filled. Then, the same coupling term as in the ARPES protocol is turned on. In this case, the second line in Eq. (A2) is not zero, however for fermions it cancels with another contribution from the second term in the first line. In total, we get for fermions

$$\begin{aligned} 1 - \langle \hat{n}_{\mathbf{q}\sigma}(t) \rangle &= t_y^2 \int_0^t dT \int_{-\tau_{\max}(T)}^{\tau_{\max}(T)} d\tau \\ &\times s\left(T - \frac{\tau}{2}\right) s\left(T + \frac{\tau}{2}\right) e^{-i(\omega - \epsilon_{\mathbf{q}} - \Delta)\tau} A_{\mathbf{q}\sigma}^>(T, \tau), \end{aligned} \quad (\text{A13})$$

i.e., in this case the hole propagation in the detection layer needs to be measured. The result involves the particle spectral function

$$A_{\mathbf{q}\sigma}^>(t_1, t_2) = \text{Tr}(\hat{\rho}_s \hat{c}_{\mathbf{q}\sigma}(t_1) \hat{c}_{\mathbf{q}\sigma}^\dagger(t_2)), \quad (\text{A14})$$

which measures the unoccupied states in the system. The same manipulations as above go through analogously to obtain the equilibrium limits and the case of a Gaussian pulse.

5. Extracting $|A|$ from two copies of the same state

Here we give an alternative protocol based on Ref. [50]. It consists in evolving two copies of the system, acting with some operators on them and interfering with them in the end.

First, prepare two copies of the same initial state $|\Psi\rangle \otimes |\Psi\rangle$ and let them evolve under the same Hamiltonian \hat{H} for time t_1 , such that we get $\exp(-i\hat{H}t_1)|\Psi\rangle \otimes \exp(-i\hat{H}t_1)|\Psi\rangle$. Then, remove a particle in the first copy at site i , evolve for time $(t_2 - t_1)$ with $t_2 > t_1$, and remove a particle in the second copy at site j . Thus, we end up in the state $\exp(-i\hat{H}(t_2 - t_1))\hat{c}_i \exp(-i\hat{H}t_1)|\Psi\rangle \otimes \hat{c}_j \exp(i\hat{H}t_2)|\Psi\rangle$. Finally, measure the swap operator SWAP by tunnel-coupling the two copies and measuring the parity-projected particle number, leading to

$$\langle \text{SWAP} \rangle_{t_1 < t_2} = |\langle \hat{c}_j^\dagger(t_2) \hat{c}_i(t_1) \rangle|^2. \quad (\text{A15})$$

APPENDIX B: RESTORING TRANSLATIONAL INVARIANCE

In the following, we show how to obtain a translationally invariant rotating frame. We show two slightly different approaches, one that leaves the initial state invariant and one that

transforms the initial state but does not contain a phase in the hopping term.

1. Without changing the initial state

We apply a time-dependent unitary transformation

$$\hat{U}(t) = \exp\left(-iBt \sum_j j \hat{S}_j^z\right), \quad (\text{B1})$$

such that the transformed Hamiltonian $\hat{H}_I + \hat{H}_B \rightarrow \hat{H}'$ is given by

$$\hat{H}' = \hat{U} \hat{H} \hat{U}^\dagger + i \frac{\partial \hat{U}}{\partial t} \hat{U}^\dagger \quad (\text{B2})$$

$$= J \sum_j \frac{1}{2} (e^{-iBt} \hat{S}_{j+1}^+ \hat{S}_j^- + e^{iBt} \hat{S}_{j+1}^- \hat{S}_j^+) + \hat{S}_{j+1}^z \hat{S}_j^z. \quad (\text{B3})$$

In this interaction picture, time evolution is governed by the Schrödinger equation

$$i \frac{d}{dt} |\psi'(t)\rangle = H'(t) |\psi'(t)\rangle, \quad (\text{B4})$$

with initial state $|\psi'(0)\rangle = \hat{U}(0)|0\rangle = |0\rangle$. Therefore, the time-evolved state in the *unrotated* frame is given by

$$|\psi_0\rangle = \hat{U}^\dagger(t_B) \mathcal{T} e^{-i \int_0^{t_B} H'(t) dt} |0\rangle. \quad (\text{B5})$$

After preparation of the state $|\psi_0\rangle$ we calculate the td-ARPES function $A_{k\sigma}(t_1, t_2) = \langle \psi_0 | \hat{c}_{k\sigma}^\dagger(t_1) \hat{c}_{k\sigma}(t_2) | \psi_0 \rangle$, which contains time evolution under the t - J model. The t - J Hamiltonian is transformed with $U(t_B)$, such that time evolution is generated by

$$\begin{aligned} \mathcal{P} \hat{H}'_{t-J} \mathcal{P} &= -t \sum_{\langle j,l \rangle, \sigma} e^{-i \frac{Bt_B}{2} (j-l)\sigma} \hat{c}_{j,\sigma}^\dagger \hat{c}_{l,\sigma} \\ &+ J \sum_j \frac{1}{2} (e^{-iBt_B} \hat{S}_{j+1}^+ \hat{S}_j^- + e^{iBt_B} \hat{S}_{j+1}^- \hat{S}_j^+) + \hat{S}_{j+1}^z \hat{S}_j^z. \end{aligned} \quad (\text{B6})$$

Moreover, we need to transform the operators $\hat{c}_{k\sigma}^\dagger$ via $\hat{U}(t_B) \hat{c}_{k,\sigma}^\dagger \hat{U}^\dagger(t_B) = \hat{c}_{k-\sigma\theta/2,\sigma}^\dagger$, such that the td-ARPES function in the laboratory frame can be written as

$$\begin{aligned} A_{k\sigma}^<(t_1, t_2) &= \langle \psi_0 | \hat{U}^\dagger(t_B) \hat{c}_{k-\sigma\theta/2,\sigma}^\dagger(t'_1) \hat{c}_{k-\sigma\theta/2,\sigma}(t'_2) \hat{U}(t_B) | \psi_0 \rangle, \end{aligned} \quad (\text{B7})$$

where we marked the times with a prime to make explicit that time evolution is done under \hat{H}'_{t-J} . Finally, inserting the time-evolved state in Eq. (B5), we can rewrite this as

$$A_{k\sigma}^<(t_1, t_2) = \langle \overline{\psi_0} | \hat{c}_{k-\sigma\theta/2,\sigma}^\dagger(t'_1) \hat{c}_{k-\sigma\theta/2,\sigma}(t'_2) | \overline{\psi_0} \rangle, \quad (\text{B8})$$

where $|\overline{\psi_0}\rangle = \mathcal{T} e^{-i \int_0^{t_B} H'(t) dt} |0\rangle$ is the ground state evolved under the rotated Hamiltonian. Using this expression, we never need to explicitly act with the unitary \hat{U} on the state.

2. Without a phase in the hopping term

For numerical reasons, we want to additionally eliminate the phase in front of the hopping term in Eq. (B6). We can do

so by shifting the unitary transformation by the corresponding constant phase, such that

$$\hat{U}(t) = \exp\left(iB(t_B - t) \sum_j j \hat{S}_j^z\right) \quad (\text{B9})$$

and

$$\begin{aligned} \hat{H}''(t) = & J \sum_j \frac{1}{2} (e^{iB(t_B-t)} \hat{S}_{j+1}^+ \hat{S}_j^- + e^{-iB(t_B-t)} \hat{S}_{j+1}^- \hat{S}_j^+) \\ & + J \sum_j \hat{S}_{j+1}^z \hat{S}_j^z. \end{aligned} \quad (\text{B10})$$

Now, the initial state in the rotated frame is given by $|\psi'(0)\rangle = \hat{U}(0)|0\rangle$, with $\hat{U}(0) = \exp(iBt_B \sum_j j \hat{S}_j^z) \neq \mathbb{1}$ such that contrary to before we need to act with a unitary on the initial state. We do this by preparing the ground state of the Hamiltonian $\hat{H}''(t=0)$ at time 0.

The other steps performed above go through as before. Notably, $U(t_B) = \mathbb{1}$, such that both the t - J Hamiltonian and the operators \hat{c}_k for the time evolution in $A_{k\sigma}(t_1, t_2)$ are unchanged. Hence, the full expression can be written as

$$A_{k\sigma}(t_1, t_2) = \langle \bar{\psi}_0 | \hat{c}_{k,\sigma}^\dagger(t_1) \hat{c}_{k,\sigma}(t_2) | \bar{\psi}_0 \rangle, \quad (\text{B11})$$

where $|\bar{\psi}_0\rangle = \mathcal{T} e^{-i \int_0^{t_B} H''(t) dt} |0''\rangle$ is the ground state of $H''(t=0)$ evolved under $H''(t)$ in Eq. (B10).

To summarize, we prepare the ground state of Hamiltonian $\hat{H}''(t=0)$, evolve it under the time-dependent Hamiltonian $\hat{H}''(t)$ until time $t = t_B$, and then calculate the spectrum according to Eq. (B11), where the time evolution is performed under the (unrotated) t - J model.

APPENDIX C: SHIFT OF SPINON OCCUPATION BY A MAGNETIC FIELD GRADIENT WITHIN CONSTRAINED FERMION MEAN-FIELD THEORY

Before deriving the spinon spectrum in a magnetic field gradient, we start with an instructive example on spinless fermions quenched by an electric field.

1. Spinless fermions in an electric field

We consider a single fermionic band in 1D in an electric field, described by the Hamiltonian

$$\hat{H} = -J \sum_i (\hat{c}_i^\dagger \hat{c}_{i+1} + \text{H.c.}) + \Delta \sum_j j \hat{n}_j. \quad (\text{C1})$$

By using the same rotating frame as in the previous Appendix, here created by unitary $\hat{U}(t) = \exp(-i\Delta(t_B - t) \sum_j j \hat{n}_j)$, the Hamiltonian in momentum space becomes

$$\hat{H}'(t) = -2J \sum_k \cos(k - \Delta(t_B - t)) \hat{c}_k^\dagger \hat{c}_k. \quad (\text{C2})$$

We then follow the same procedure as in the t - J model: We prepare the ground state of $\hat{H}'(t)$ at time $t = 0$, given by

$$|0\rangle = \prod_{|k-\Delta t_B| \leq k_F} \hat{c}_k^\dagger |0\rangle, \quad (\text{C3})$$

where k_F is the Fermi momentum in the absence of a tilt. The time evolution of this state under the time-dependent

Hamiltonian \hat{H}' until time t_B can be calculated by noting that $\hat{c}_k^\dagger(t_B) = \exp(-2Ji \int_0^{t_B} \cos(k - \Delta(t_B - t')) dt') \hat{c}_k^\dagger$, and hence

$$|\bar{\psi}_0\rangle \equiv \mathcal{T} \exp\left(-i \int_0^{t_B} \hat{H}'(t') dt'\right) |0\rangle \quad (\text{C4})$$

$$= \prod_{|k-\Delta t_B| \leq k_F} \exp\left(-\frac{2Ji}{\Delta} [\sin(k) - \sin(k - \Delta t_B)]\right) \hat{c}_k^\dagger |0\rangle. \quad (\text{C5})$$

The ARPES spectrum then follows as

$$A_k(\omega) \equiv \int d(t_1 - t_2) e^{i\omega(t_1 - t_2)} \langle \bar{\psi}_0 | \hat{c}_k^\dagger(t_1) \hat{c}_k(t_2) | \bar{\psi}_0 \rangle \quad (\text{C6})$$

$$= 2\pi \delta(\omega - 2J \cos(k)) \langle \bar{\psi}_0 | \hat{c}_k^\dagger \hat{c}_k | \bar{\psi}_0 \rangle \quad (\text{C7})$$

$$= 2\pi \delta(\omega - 2J \cos(k)) \Theta(|k - \Delta t_B| - k_F). \quad (\text{C8})$$

This result shows some of the main features of the numerical results for the t - J model in a gradient magnetic field: One can scan along the whole dispersion by changing Δt_B , occupying states that are not occupied in the ground state without the field. However, in contrast to the t - J model, the result is independent of both the central time $t_1 + t_2$ and the strength of the tilt field Δ . Furthermore, the above result can be easily generalized to spinful fermions in a magnetic field gradient: they just get shifted in opposite directions by $\pm \Delta t_B/2$, where the factor of one-half comes from the fact that $\hat{S}^z = \frac{1}{2}(\hat{n}_\uparrow - \hat{n}_\downarrow)$.

2. Spinon mean-field theory

Here we show that the magnetic field gradient protocol leads to a shift of the occupation of the spinon dispersion. We start from the Heisenberg model in a magnetic field gradient,

$$H = J \sum_i \frac{1}{2} (S_i^+ S_{i+1}^- + S_i^- S_{i+1}^+) + \hat{S}_i^z \hat{S}_{i+1}^z - B \sum_j j \hat{S}_j^z. \quad (\text{C9})$$

Introducing constrained fermion operators by $\hat{S}_i^\pm = \hat{f}_{i\uparrow}^\dagger \hat{f}_{i\downarrow}$, $\hat{S}_i^z = \frac{1}{2}(\hat{f}_{i\uparrow}^\dagger \hat{f}_{i\uparrow} - \hat{f}_{i\downarrow}^\dagger \hat{f}_{i\downarrow})$ with constraint $\sum_\alpha \hat{f}_{i,\alpha}^\dagger \hat{f}_{i,\alpha} = 1$, we get

$$\begin{aligned} \hat{H} = & -\frac{J}{2} \sum_{i,\alpha} \hat{f}_{i,\alpha}^\dagger \hat{f}_{i+1,\alpha} (f_{i+1,\bar{\alpha}}^\dagger \hat{f}_{i,\bar{\alpha}} + f_{i+1,\alpha}^\dagger \hat{f}_{i,\alpha}) \\ & - \frac{B}{2} \sum_\alpha \alpha \sum_j j \hat{f}_{j\alpha}^\dagger \hat{f}_{j\alpha}. \end{aligned} \quad (\text{C10})$$

Here, we defined $\alpha = +/ -$ for \uparrow / \downarrow and $\bar{\uparrow} = \downarrow$, $\bar{\downarrow} = \uparrow$. Moreover, we neglected all constant terms.

To decouple the interactions, we introduce a spin-dependent mean field

$$\chi_\alpha = \langle \hat{f}_{i,\alpha}^\dagger \hat{f}_{i+1,\alpha} \rangle \quad (\text{C11})$$

and neglect all terms quadratic in the fluctuations around this mean field, arriving at

$$\begin{aligned} \hat{H} = & -\frac{JL}{2} \sum_\alpha \chi_\alpha (\chi_{\bar{\alpha}}^\dagger + \chi_\alpha^\dagger) \\ & - \frac{J}{2} \sum_{i,\alpha} ((\chi_\alpha + \chi_{\bar{\alpha}}) \hat{f}_{i+1,\alpha}^\dagger \hat{f}_{i,\alpha} + \text{H.c.}) \end{aligned}$$

$$-\frac{B}{2} \sum_{\alpha} \alpha \sum_j j \hat{f}_{j\alpha}^{\dagger} \hat{f}_{j\alpha}. \quad (\text{C12})$$

To follow the protocol, we move into the rotating frame of the magnetic field gradient with the unitary

$$\hat{U} = \exp\left(i\frac{B}{2}(t_B - t) \sum_{\alpha} \alpha \sum_j j \hat{f}_{j\alpha}^{\dagger} \hat{f}_{j\alpha}\right), \quad (\text{C13})$$

such that

$$\hat{f}_{j\alpha} \rightarrow U \hat{f}_{j\alpha} U^{\dagger} = \exp\left(-i\frac{\alpha B j}{2}(t_B - t)\right) \hat{f}_{j,\alpha}. \quad (\text{C14})$$

Defining $f_j = \frac{1}{\sqrt{L}} \sum_k e^{-ikj} f_k$, and taking the infinite system size limit $(1/L) \sum_k = (1/2\pi) \int dk$, the Hamiltonian density becomes

$$\begin{aligned} \hat{H}(t) = & -\frac{JL}{2} \sum_{\alpha} \chi_{\alpha}(t) [\chi_{\bar{\alpha}}^{\dagger}(t) + \chi_{\alpha}^{\dagger}(t)] \\ & + \int_{-\pi}^{\pi} dk \sum_{\alpha} \epsilon_{\alpha}(k, t) \hat{f}_{k\alpha}^{\dagger} \hat{f}_{k\alpha} \end{aligned} \quad (\text{C15})$$

with dispersion

$$\epsilon_{\alpha}(k, t) = -\frac{J}{2} ((\chi_{\alpha} + \chi_{\bar{\alpha}}) e^{i[k + \frac{\alpha B}{2}(t_B - t)]} + \text{c.c.}). \quad (\text{C16})$$

Moreover, using that in the ground state $\langle \hat{f}_k^{\dagger} \hat{f}_{k'} \rangle \sim \delta_{kk'}$, the mean field transforms to

$$\chi_{\alpha}(t) = \frac{1}{2\pi} \int_{-\pi}^{\pi} dk e^{-i[k + \frac{\alpha B}{2}(t_B - t)]} \langle \hat{f}_{k,\alpha}^{\dagger} \hat{f}_{k,\alpha} \rangle. \quad (\text{C17})$$

To find the ground-state solution for $t = 0$, we need to minimize $\langle \hat{H} \rangle$ self-consistently under the constraint (C17). To

do so, we set the phase of $\chi_{\alpha} + \chi_{\bar{\alpha}}$ to zero (without loss of generality as the ground state is degenerate with respect to this phase) such that

$$\epsilon_{\alpha}(k, t = 0) = -J \left[|\chi_{\alpha} + \chi_{\bar{\alpha}}| \cos\left(k + \frac{\alpha B}{2} t_B\right) \right]. \quad (\text{C18})$$

The ground state is hence given by a Fermi sea with the Fermi momenta given by $|k_F + \alpha \frac{B}{2} t_B| = \frac{\pi}{2}$. Inserting this into (C17), we find

$$\chi_{\alpha}(t = 0) = \frac{1}{2\pi} \int_{(-\pi - \alpha B t_B)/2}^{(\pi - \alpha B t_B)/2} dk e^{-i(k + \frac{\alpha B}{2} t_B)} \quad (\text{C19})$$

$$= \frac{1}{\pi} \quad (\text{C20})$$

independent of α , and we get our final result for the spinon dispersion,

$$\epsilon_{\alpha}(k, t = 0) = -\frac{2J}{\pi} \cos\left(k + \frac{\alpha B}{2} t_B\right). \quad (\text{C21})$$

Having found the ground state at $t = 0$, we can now proceed with time evolving the state until $t = t_B$ to then calculate the spinon spectral function as in the previous example for free fermions, yielding

$$A_{k,\alpha}^S(\omega) \equiv \int d(t_1 - t_2) e^{i\omega(t_1 - t_2)} \langle \psi_0 | \hat{f}_k^{\dagger}(t_1) \hat{f}_k(t_2) | \psi_0 \rangle \quad (\text{C22})$$

$$= 2\pi \delta\left(\omega + \frac{2J}{\pi} \cos(k)\right) \Theta\left(|k + \alpha B t_B / 2| - \frac{\pi}{2}\right). \quad (\text{C23})$$

-
- [1] J. G. Bednorz and K. A. Müller, *Z. Phys. B* **64**, 189 (1986).
[2] A. Damascelli, Z. Hussain, and Z.-X. Shen, *Rev. Mod. Phys.* **75**, 473 (2003).
[3] K. M. Shen, F. Ronning, D. H. Lu, F. Baumberger, N. J. C. Ingle, W. S. Lee, W. Meevasana, Y. Kohsaka, M. Azuma, M. Takano, H. Takagi, and Z.-X. Shen, *Science* **307**, 901 (2005).
[4] S. Sachdev and D. Chowdhury, *Prog. Theor. Exp. Phys.* **2016**, 12C102 (2016).
[5] J. M. Luttinger, *Phys. Rev.* **119**, 1153 (1960).
[6] M. Oshikawa, *Phys. Rev. Lett.* **84**, 3370 (2000).
[7] A. F. Kemper, M. Sentef, B. Moritz, C. C. Kao, Z. X. Shen, J. K. Freericks, and T. P. Devereaux, *Phys. Rev. B* **87**, 235139 (2013).
[8] N. Bittner, D. Golež, H. U. R. Strand, M. Eckstein, and P. Werner, *Phys. Rev. B* **97**, 235125 (2018).
[9] Y. Murakami, S. Takayoshi, A. Koga, and P. Werner, *Phys. Rev. B* **103**, 035110 (2021).
[10] A. Schuckert and M. Knap, *Phys. Rev. Research* **2**, 043315 (2020).
[11] M. Babadi, M. Knap, I. Martin, G. Refael, and E. Demler, *Phys. Rev. B* **96**, 014512 (2017).
[12] C. Giannetti, M. Capone, D. Fausti, M. Fabrizio, F. Parmigiani, and D. Mihailovic, *Adv. Phys.* **65**, 58 (2016).
[13] C. L. Smallwood, R. A. Kaindl, and A. Lanzara, *Europhys. Lett.* **115**, 27001 (2016).
[14] D. Fausti, R. I. Tobey, N. Dean, S. Kaiser, A. Dienst, M. C. Hoffmann, S. Pyon, T. Takayama, H. Takagi, and A. Cavalleri, *Science* **331**, 189 (2011).
[15] L. Perfetti, P. A. Loukakos, M. Lisowski, U. Bovensiepen, H. Eisaki, and M. Wolf, *Phys. Rev. Lett.* **99**, 197001 (2007).
[16] M. A. Nichols, L. W. Cheuk, M. Okan, T. R. Hartke, E. Mendez, T. Senthil, E. Khatami, H. Zhang, and M. W. Zwierlein, *Science* **363**, 383 (2019).
[17] T.-L. Dao, A. Georges, J. Dalibard, C. Salomon, and I. Carusotto, *Phys. Rev. Lett.* **98**, 240402 (2007).
[18] J. T. Stewart, J. P. Gaebler, and D. S. Jin, *Nature (London)* **454**, 744 (2008).
[19] P. T. Brown, E. Guardado-Sanchez, B. M. Spar, E. W. Huang, T. P. Devereaux, and W. S. Bakr, *Nat. Phys.* **16**, 26 (2019).
[20] M. Ben Dahan, E. Peik, J. Reichel, Y. Castin, and C. Salomon, *Phys. Rev. Lett.* **76**, 4508 (1996).
[21] P. M. Preiss, R. Ma, M. E. Tai, A. Lukin, M. Rispoli, P. Zupancic, Y. Lahini, R. Islam, and M. Greiner, *Science* **347**, 1229 (2015).
[22] F. Meinert, M. Knap, E. Kirilov, K. Jag-Lauber, M. B. Zvonarev, E. Demler, and H.-C. Naegerl, *Science* **356**, 945 (2017).

- [23] G. Ji, M. Xu, L. Haldar Kendrick, C. S. Chiu, J. C. Brüggengjürgen, D. Greif, A. Bohrdt, F. Grusdt, E. Demler, M. Lebrat, and M. Greiner, *Phys. Rev. X* **11**, 021022 (2021).
- [24] J. Koepsell, D. Bourgund, P. Sompet, S. Hirthe, A. Bohrdt, Y. Wang, F. Grusdt, E. Demler, G. Salomon, C. Gross, and I. Bloch, *Science* **374**, 82 (2021).
- [25] E. Guardado-Sanchez, A. Morningstar, B. M. Spar, P. T. Brown, D. A. Huse, and W. S. Bakr, *Phys. Rev. X* **10**, 011042 (2020).
- [26] T. Giamarchi, *Quantum Physics in One Dimension*, International Series of Monographs on Physics (Clarendon, Oxford, United Kingdom, 2003).
- [27] T. A. Hilker, G. Salomon, F. Grusdt, A. Omran, M. Boll, E. Demler, I. Bloch, and C. Gross, *Science* **357**, 484 (2017).
- [28] J. Vijayan, P. Sompet, G. Salomon, J. Koepsell, S. Hirthe, A. Bohrdt, F. Grusdt, I. Bloch, and C. Gross, *Science* **367**, 186 (2020).
- [29] C. Kim, A. Y. Matsuura, Z.-X. Shen, N. Motoyama, H. Eisaki, S. Uchida, T. Tohyama, and S. Maekawa, *Phys. Rev. Lett.* **77**, 4054 (1996).
- [30] A. Bohrdt, D. Greif, E. Demler, M. Knap, and F. Grusdt, *Phys. Rev. B* **97**, 125117 (2018).
- [31] A. Bohrdt, E. Demler, F. Pollmann, M. Knap, and F. Grusdt, *Phys. Rev. B* **102**, 035139 (2020).
- [32] J. K. Freericks, H. R. Krishnamurthy, and T. Pruschke, *Phys. Rev. Lett.* **102**, 136401 (2009).
- [33] B. Moritz, T. P. Devereaux, and J. K. Freericks, *Phys. Rev. B* **81**, 165112 (2010).
- [34] S. Gupta, Z. Hadzibabic, M. W. Zwierlein, C. A. Stan, K. Dieckmann, C. H. Schunck, E. G. M. van Kempen, B. J. Verhaar, and W. Ketterle, *Science* **300**, 1723 (2003).
- [35] M. Greiner, C. A. Regal, and D. S. Jin, *Phys. Rev. Lett.* **94**, 070403 (2005).
- [36] M. Cetina, M. Jag, R. S. Lous, I. Fritsche, J. T. M. Walraven, R. Grimm, J. Levinsen, M. M. Parish, R. Schmidt, M. Knap, and E. Demler, *Science* **354**, 96 (2016).
- [37] J. B. Pendry, *Phys. Rev. Lett.* **45**, 1356 (1980).
- [38] G. Baskaran, Z. Zou, and P. Anderson, *Solid State Commun.* **63**, 973 (1987).
- [39] P. Coleman, *Phys. Rev. B* **29**, 3035 (1984).
- [40] M. Ogata and H. Shiba, *Phys. Rev. B* **41**, 2326 (1990).
- [41] X.-G. Wen, *Quantum Field Theory of Many-body Systems* (Oxford University Press, Oxford, 2004).
- [42] R. Eder and Y. Ohta, *Phys. Rev. B* **56**, 2542 (1997).
- [43] R. N. Bannister and N. d'Ambrumenil, *Phys. Rev. B* **61**, 4651 (2000).
- [44] See Supplemental Material at <http://link.aps.org/supplemental/10.1103/PhysRevB.104.235107> for a video showing the time evolution in Fig. 3 in more detail.
- [45] A. Keselman, L. Balents, and O. A. Starykh, *Phys. Rev. Lett.* **125**, 187201 (2020).
- [46] F. Ferrari and F. Becca, *Phys. Rev. B* **98**, 100405(R) (2018).
- [47] A. M. Black-Schaffer and C. Honerkamp, *J. Phys.: Condens. Matter* **26**, 423201 (2014).
- [48] H. Petek and S. Ogawa, *Prog. Surf. Sci.* **56**, 239 (1997).
- [49] M. Aidelsburger, M. Atala, S. Nascimbene, S. Trotzky, Y. A. Chen, and I. Bloch, *Phys. Rev. Lett.* **107**, 255301 (2011).
- [50] A. Bohrdt, C. B. Mendl, M. Endres, and M. Knap, *New J. Phys.* **19**, 063001 (2017).